Mobile Netw Appl (2010) 15:461–474
DOI 10.1007/s11036-009-0199-9

Lessons Learned from an Extensive Spectrum Occupancy Measurement Campaign and a Stochastic Duty Cycle Model

Matthias Wellens · Petri Mähönen

Published online: 15 August 2009

Abstract Several measurement campaigns have shown that numerous spectrum bands are vacant although licenses have been issued by the regulatory agencies. Dynamic spectrum access (DSA) has been proposed in order to alleviate this problem and increase the spectral utilization. In this paper we present our spectrum measurement setup and discuss lessons learned during our measurement activities. We compare measurement results gathered at three locations and show differences in the background noise processes. Additionally, we introduce a new model for the duty cycle distribution that has multiple applications in the DSA research. We point out that fully loaded and completely vacant channels should be modelled explicitly and discuss the impact of duty cycle correlation in the frequency domain. Finally, we evaluate the efficiency of an adaptive spectrum sensing process as an example for applications of the introduced model.

Keywords wireless communication · dynamic spectrum access · spectrum measurements · spectrum modelling · duty cycle modelling

1 Introduction

Recently, dynamic spectrum access (DSA) technologies have attracted significant interest in the research community, see, e.g., [2, 35] and references therein. Mainly three facts have been the motivation for this work. First, the scarcity of radio spectrum complicates the process of allocating spectrum to new wireless systems. Second, the success of wireless communication and the trend towards broadband systems further increases the need for radio spectrum. Third, researchers have found that significant amount of officially licensed radio spectrum is unused. This has been reported based on several extensive spectrum occupancy measurement campaigns [3, 4, 8, 12, 15, 16, 20–22, 24, 27, 28, 34].

DSA-capable systems sense the radio environment around them, try to identify unused frequency bands, so called spectrum white spaces, and opportunistically use those without causing harmful interference to the primary users.[1] Therefore, these devices are capable of changing their working frequency and bandwidth [6]. This flexibility, together with the spectrum sensing, enables DSA systems to alleviate or even solve the spectrum scarcity problem. More efficient use of spectral resources has also the potential to reduce costs and improve reliability of wireless systems. However, the added degrees of freedom increase the system complexity and more adaptive and intelligent devices are required to ensure efficient system operation. The cognitive radio vision [14, 17], which describes devices that are aware of their surroundings and that adapt accordingly, has been introduced as potential solution to this challenge.

M. Wellens (✉) · P. Mähönen
Department of Wireless Networks, RWTH Aachen University, Kackertstrasse 9, 52072 Aachen, Germany
e-mail: mwe@mobnets.rwth-aachen.de

P. Mähönen
e-mail: pma@mobnets.rwth-aachen.de

[1] A primary user denotes a system possessing the license to access a frequency band. The systems accessing spectrum white spaces opportunistically are called secondary users [6]. Primary users are often also called incumbent users.

Both, the DSA as well as the cognitive radio research, require realistic models and good understanding of the current networks as basis for performance evaluation. In this context, the contributions of this paper are twofold. First, we describe in detail our spectrum measurements and lessons learned during the extensive measurement campaign. Enhanced measurement methodology is crucial for obtaining reliable results and the design of appropriate models. Second, we introduce a model for the distribution of the duty cycle of several wireless systems. Such models are required for the evaluation of multiple aspects of DSA-capable systems. Adaptive sensing approaches are one example and those have been shown to significantly improve spectrum sensing efficiency [11, 30, 31]. Another use case is the evaluation of adaptive multicarrier systems that are able to suppress few subcarriers and limit adjacent channel interference in order not to harm primary system transmissions [5, 10, 23]. Additionally, we also present a short evaluation of the correlation of the duty cycle over frequency.

We chose the adaptive spectrum sensing use case in order to illustrate the applicability of the developed model to relevant research problems. We show that using spectrum sensing statistics can significantly improve the efficiency of spectrum sensing. We compare the results when examining adaptive sensing algorithms using different spectrum models and point out that less accurate models may result in misleading conclusions. Our model reproduces several of the key characteristics of spectrum use but, at the same time, keeps the model complexity at a reasonable level.

We combine the measurement results and the duty cycle model in one paper since spectrum modelling is closely connected to the underlying measurement methodology. Vector signal analysis, as deployed, e.g., by Geirhofer et al. [13], enables detailed analysis of a single signal on a per-symbol basis but is strictly limited in the covered bandwidth. In contrast, swept spectrum analysis supports wideband measurements at the price of a significantly lower sampling rate. Both approaches can cover only some aspects of spectrum usage. Therefore, a detailed description of the deployed measurement methodology enables better understanding of the extracted model and appropriate use by the community later on.

This paper is an extension of a previous version [32] and includes further additions and enhancements to the existing results. In [32] the whole measurement traces have been analysed for the duty cycle modelling. Here, we use specifically chosen subtraces in order to provide more realistic model parameters that describe spectrum use during the most important time periods during the day. Due to the evaluation of different data subsets the reported model parameters differ from those listed in [32]. Furthermore, the evaluation methods of the model accuracy have been improved. We also added an important application of the model in order to show its direct applicability for problems in the DSA area.

The rest of the paper is structured as follows. We start in Section 2 with the description of the measurement setup and comment on lessons learned during our measurement campaign. We compare the results collected at different measurement locations in Section 3 and discuss the modelling of the duty cycle in Section 4. In Section 5 we examine adaptive spectrum sensing as an application area of our introduced model. Finally, we conclude the paper in Section 6.

2 Spectrum measurement setup

We start this section with the detailed description of our measurement setup followed by some comments on which measurement locations we have selected. We give rationale for most of our design decisions and include comments on insights that we have gained throughout our campaign.

2.1 Hardware components and system configuration

One of the major goals of our measurement campaign was to investigate changes of spectrum usage over longer time scales of multiple days to few weeks. Since wireless systems have different characteristics in terms of used bandwidth, multiple access scheme, transmit power etc., engineers often choose measurement parameters optimized for the investigated system, see, e.g., [12, 20–22]. Assuming a limited period of time for the complete measurement campaign, the required reconfigurations of the measurement setup reduce either the number of technologies, which can be examined in a time division fashion, or shorten the available measurement time per technology. Instead, we decided to inspect multiple technologies in parallel with partially suboptimal measurement configuration. In detail, we examined 1.5 GHz wide subbands with a resolution bandwidth of 200 kHz. Thus, the chosen frequency resolution is not fine enough to differentiate very narrowband primary user signals.

In total we measured the frequency range from 20 MHz up to 6 GHz where most wireless services work today. Due to the general trend in wireless communication towards more broadband applications we also expect DSA networks to be broadband systems. Although multicarrier systems are able to suppress

intermediate subcarriers and benefit also from non-continuous spectrum white spaces, we still assume that also from an application point of view spectrum white spaces of few tens of kHz are not interesting for opportunistic use and the rather coarse resolution bandwidth of 200 kHz represents a good compromise.

In the following we will comment on each component of our measurement setup in more detail. We list the detailed set of used measurement parameters in Table 1 and Fig. 1 shows the complete measurement setup.

As mentioned above, we designed a very wideband measurement setup and this main characteristic drastically limited the selection of standard off-the-shelf components. Specially designed modules were no alternative due to the high costs of such bespoke solutions. In contrast, focusing the measurements on a single, mass-market technology such as any cellular technology would greatly increase the amount of available components and especially ease the selection of affordable antennas and amplifiers.

We used three different antennas each specifically selected for a certain frequency band. A large discone antenna of type *AOR DA-5000* covered the lowest frequency band between 20 MHz and 1.52 GHz. We deployed a smaller discone antenna of type *AOR DA-5000JA* to receive signals in the next subband from 1.5 GHz up to 3 GHz. Finally, we used a radom antenna of type *Antennentechnik Bad Blankenburg AG KS 1-10* specified up to 10 GHz to cover the frequency range between 3 GHz and 6 GHz. The antennas are vertically polarized, have an omnidirectional characteristic in the horizontal plane, and are slightly directive in the vertical plane. Other researchers have used horizontally directive antennas, see, e.g., [16, 20–22], but our choice avoids the need for further reconfiguration of the measurement setup to cover all possible directions.

Table 1 Spectrum analyzer configuration used throughout the measurements

Center frequency	Band 1: $f_c = 770$ MHz Band 2: $f_c = 2250$ MHz Band 3: $f_c = 3750$ MHz Band 4: $f_c = 5250$ MHz
Frequency span	1500 MHz
Resolution bandwidth	200 kHz
Number of measurement points	8192
Sweep time	1 s
Measurement duration	About 7 days per subband
Detector type	Average detector
Preamplifier	Up to 3 GHz: 28 dB gain, above 3 GHz: none or $\geq$ 24 dB gain
Instrument	Agilent E4440A spectrum analyzer
Typical DANL (displayed average noise level)	−169 dBm [1] at 1 GHz and 1 Hz resolution bandwidth

Fig. 1 Measurement setup as it was deployed on the roof of the International School Maastricht, Maastricht, Netherlands

In order to ensure a sufficiently sensitive measurement system we preamplified nearly all incoming signals and limited the required length of interconnecting cables by deploying the measurement instrument inside a weather-proof box next to the antennas. We always preamplified signals up to 3 GHz using the preamplifier inbuilt in the spectrum analyzer. At some locations we added an external preamplifier to further increase the sensitivity of the measurement setup also for frequencies above 3 GHz.

The selection of the measurement device will very often be restricted by the availability of instruments or limited funding for new equipment. However, in the spectrum occupancy context special attention should be paid to the sensitivity of the device. If the setup has to be portable or access to electrical power is otherwise limited, after careful analysis a compromise between portability and measurement sensitivity might also have to be accepted. Portable devices often do not allow similarly high number of measurement points, another rather unusual requirement of very wideband measurements, or do not support flexible data exchange

via Ethernet. We used a high performance spectrum analyzer Agilent E4440A, which supports up to 8192 measurement points. Based to the bandwidth characteristics of the selected antennas and the fact that several popular wireless systems, e.g., FM radio or GSM,[2] use channels of 200 kHz bandwidth, we have selected the above introduced parameters for frequency span and resolution bandwidth.

We chose the sweep time to be 1 sec as a compromise between the amount of data, that is collected throughout one week of measurement, the variance of the gathered samples due to noise variation, and the sampling frequency. Present wireless systems use too short frames or time slots as to allow a wideband measurement setup to sample each one. Additionally, the spectrum analyzer periodically realigns the internal calibration, which pauses the measurement for usually few seconds.

We measured the spectrum usage in each of the four subbands for about seven days at each location. In some cases we lowered the measurement duration for the highest subbands to few days and at one location we also measured the second subband for 14 days. Taking in account the spectrum analyzer recalibrations, a measurement of one week results in a measurement trace of about 335000 sweeps (on average each sweeps takes 1.8 s and 1000 sweeps take about 30 min).

We used a standard laptop for automatic instrument configuration and data saving purposes. It remote controlled the analyzer via Ethernet using standard protocols for instrument control. On the software side usually flexibility in measurement configuration and quick access to first analysis and visualization results are important because they enable prevalidation of the recorded data at the measurement site. In our case, the deployed Virtual Instrument Software Architecture (VISA) library enabled convenient development of high-level MATLAB software focused on the efficient data gathering and analysis.

Finally, we installed all components in a weatherproof wooden but RF-shielded box. The box also enabled us to fix the measurement setup at very exposed and windy locations. Although we ran measurements for multiple weeks we did not add lightning protection. The two major reasons against are the limited availability of very wideband lightning protection components and the additional logistics. Proper protection of the measurement setup requires access to the lightning protection system of the building, which was restricted at some locations. Instead, we closely followed the weather forecast and would have taken down the setup in case of high probability of thunderstorms. More permanent setups at exposed sites definitely require lightning protection, as discussed, e.g., in [3, 26].

We also monitored the temperature and humidity inside the measurement box using the sensors on a Telos mote [25]. Although we were concerned about dew in the morning hours the humidity turned out to be no problem. During some measurements in summer the temperature inside the box significantly increased and caused stability problems due to the operation of the spectrum analyzer outside its specifications. We drilled additional holes to the wooden box and added fans for cooling that solved the problem without increasing the humidity inside the box to critical levels.

The final weather problem we faced was snow fall. During some of the measurements in winter time, snow on the antenna radically changed the reception characteristics of the large discone. Since in Aachen only limited amount of snow falls during winter time we did not investigate the problem further, but a sharp drop in the measured power spectral density (*PSD*) shows high correlation to the time period during which the temperatures have been low enough to prevent the snow from melting.

Table 2 Measurement locations

Name	Short name	Short description
Aachen, indoor	IN	Modern office building in Aachen, Germany
Netherlands	NE	Rooftop location in a mostly residential area in Maastricht, Netherlands
Aachen, balcony	AB	Third floor balcony of a residential building in a rather central housing area of Aachen, Germany

2.2 Measurement locations

We report about measurements taken at three different locations. The first measurements were performed indoor in a room located in the ground floor of a modern office building in Aachen, Germany.[3] In order to investigate also other frequency regulations we selected a location in the Netherlands as second reference location. We placed our measurement box on the roof of the

[2] Global System for Mobile Communication (GSM).

[3] IN: Latitude: 50° 47′ 24.01″ North, Longitude: 6° 3′ 47.42″ East.

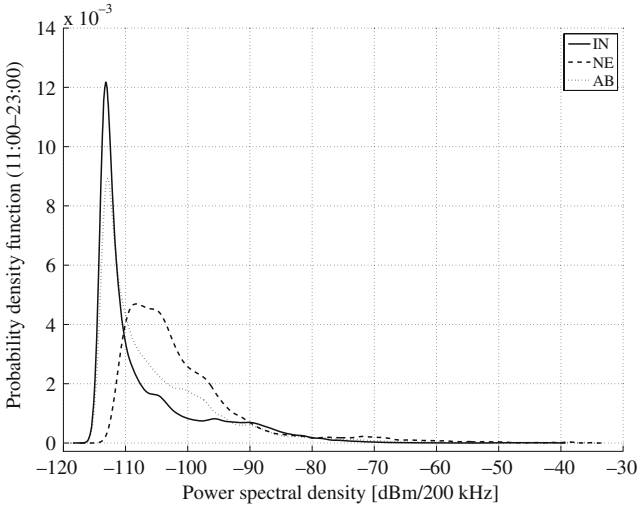

Fig. 2 Comparison of the probability density function of the power spectral density samples collected in the first subband ($f \in [20, 1520]$ MHz) at all measurement locations over 12 h (11:00–23:00) during different normal weekdays

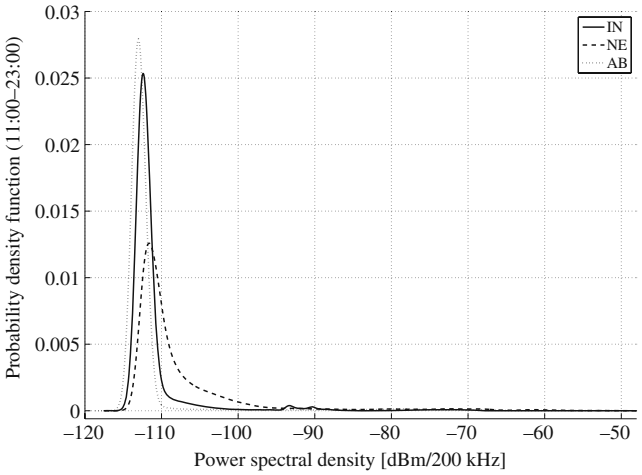

Fig. 3 Comparison of the probability density function of the power spectral density samples collected in the second subband ($f \in [1500, 3000]$ MHz) at all measurement locations over 12 h (11:00–23:00) during different normal weekdays

main building of the International School Maastricht.[4] We chose the third location as an example for locations where end-user devices capable of dynamic spectrum access might work in real scenarios. We measured the spectrum usage on a third-floor balcony of an older residential building in a rather central housing area of Aachen.[5] For reference, we list all locations in Table 2.

3 Comparison of measurement locations

Before we present detailed results on the modelling of the duty cycle in Section 4 we compare the power spectral density (*PSD*) measured at the different locations. As a first example we discuss the probability density function (PDF) of all measured *PSD* samples received in the first subband. Due to the large amount of data and the differences between day- and nighttime we limit the analysis to twelve hours during daytime. We validated that we can compare the results between locations to a certain extend although we gathered them at different dates. We compared separate parts of the data measured at the same location. Since we did not find very significant differences, comparison of high level statistics is reasonable. Figure 2 shows the PDF for all locations.

All shown distributions are asymmetric and can be interpreted as consisting of two components. First, a large fraction of the received samples belongs to a background noise process. Second, most of the samples with higher power belong to real-life transmissions and cause the asymmetry of the density function. Both components are different at every location.

The samples of the second component, the real-life signals, are stronger at the more exposed location in the Netherlands. This was to be expected because of the presence of line-of-sight (LOS) connections and the lower pathloss at the rooftop location. However, also the background noise process is stronger at the exposed location. Only at the indoor location IN and in the calm radio environment at AB, the noise process shows similar characteristics as we measured with a 50 Ω fitted match in our laboratory. At the third location man-made noise results in stronger background noise and an increased minimum *PSD*. Additionally, the variance of the background noise process evaluated over the frequency channels is higher at the more exposed location.

The PDF plot for the second subband at $f_c = 2250$ MHz looks similar as shown in Fig. 3. The asymmetry is less pronounced because less primary user systems are active. Several major services such as the GSM1800 or the Universal Mobile Telecommunications System (UMTS) operate in this spectrum band and also the ISM-band[6] at 2.4 GHz is often busy but apart from these very popular services significantly

[4]NE: Latitude: 50° 50’ 32.34" North, Longitude: 5° 43′ 14.93″ East.

[5]AB: Latitude: 50° 46′ 8.90″ North, Longitude: 6° 4′ 42.59″ East.

[6]The ISM-band is reserved for industrial, scientific, and medical applications.

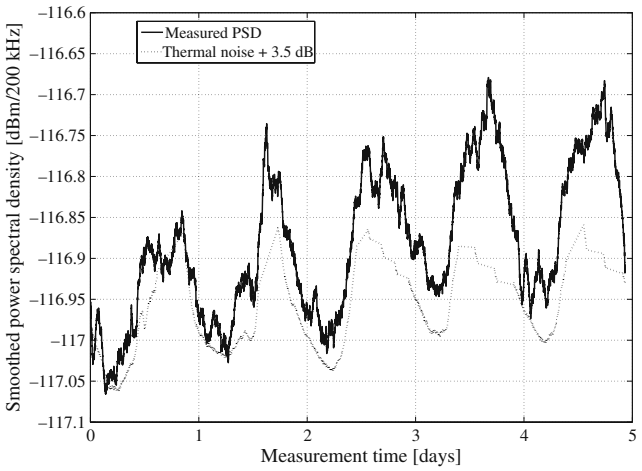

Fig. 4 Comparison of measured *PSD* and thermal background noise at $f = 4$ GHz as measured at the location in the Netherlands. The measured *PSD* was smoothed over 2000 samples (about one hour of measurement time) in order to enable a clear visualization of the underlying trend. The thermal noise was moved up by 3.5 dB in order to enable more direct comparison. Each tick on the x-axes marks midnight

less usage compared to the lower spectrum band was detected by our measurement setup. Again, the background noise process is stronger at the more exposed measurement location in the Netherlands.

We also measured considerably less signals in the two highest subbands (3–4.5 GHz and 4.5–6 GHz). The setup detected only a handful of signals above −100 dBm/200 kHz at all locations. Although the deployed antenna is probably less sensitive due to its very wideband nature we can still conclude that the frequency range above 3 GHz is much less crowded compared to the lower frequency ranges.

Figure 4 shows the *PSD* measured over five days at the high frequency $f = 4$ GHz at which we did not detect any primary transmitter. The data were gathered at NE using the additional preamplifier that further improves the sensitivity of the measurement setup. The figure also shows the thermal background noise computed based on the Boltzmann constant, the resolution bandwidth, and the temperature measured by the Telos mote.[7] We smoothed the measured *PSD* in order to clearly show the trend and the cycle of day and night. Additionally, we moved up the thermal noise by 3.5 dB for direct comparison of both graphs.

Although we received only a small amount of background noise at such high frequencies the difference between thermal noise and received signal strength is still higher during the day time compared to the night time. This result confirms that the received noise is man-made due to its similar 24 h-cycle as present in several other wireless systems today [30, 31].

[7]For few samples the data transfer from the mote to the laptop failed but the slow changing temperature is still sufficiently described.

4 Duty cycle modelling

In this Section we will introduce a stochastic model for the distribution of the duty cycle based on the 200 kHz channelization that we used throughout our measurement campaign.

Since we measured multiple different frequency bands allocated to various wireless systems we apply generic energy detection [2, 7] based on the detection threshold γ. We use different threshold values in order to address the different background noise levels and achieve realistic estimates of the duty cycle. The lowest threshold is $\gamma = -107$ dBm as given for 200 kHz channels in an earlier requirements document of the IEEE 802.22 standardization committee [29]. Additionally, we evaluate few higher threshold values.

Let $\Omega_{t,i}$ denote the spectrum occupancy at time index t and channel index i, defined as

$$\Omega_{t,i} = \begin{cases} 0 \text{ if } PSD_{rx,t,i} < \gamma \\ 1 \text{ if } PSD_{rx,t,i} \geq \gamma \end{cases}, \tag{1}$$

where $PSD_{rx,t,i}$ is the received *PSD* measured in channel i and at time index t. If $\Omega_{t,i} = 1$ a primary user signal is detected and the channel is *occupied*. *PSD* values below γ indicate a *free* channel, respectively. Furthermore, let us denote S_i as the number of measured samples in channel i and DC_i as the duty cycle computed for channel i:

$$DC_i = \frac{\sum_{t=1}^{S_i} \Omega_{t,i}}{S_i}. \tag{2}$$

4.1 Distribution of the duty cycle

We are now interested in the distribution of DC_i over all channels i that belong to a certain subband. That may be a complete subband covered in one measurement but may also be a subband allocated to a specific group of wireless services such as the ISM-band.

We do not evaluate the full traces measured during multiple consecutive days but focus our analysis on representative subtraces that describe the spectrum occupancy during daytime. We compared the distributions for the busy and idle time period durations between all measurement days and selected typical examples. We used the same subtraces as for the *PSD* analysis discussed in Section 3. The examined time periods last

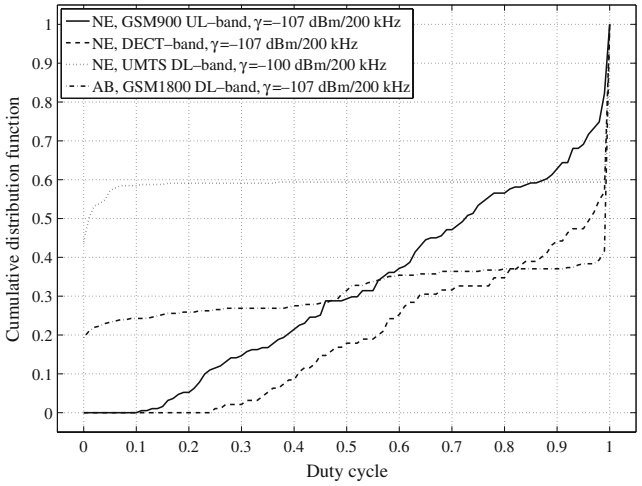

Fig. 5 Comparison of different duty cycle distributions based on measurements taken at NE and AB using appropriate thresholds

from 11:00 in the morning to 23:00 in the evening. Further details on the time period selection procedure have been given in [33].

After application of the energy detection we estimate the cumulative distribution function (CDF) of the duty cycle DC_i and compute the PDF by simple differencing.[8]

Figure 5 shows few selected examples for the CDF. The slope of most CDF graphs is the highest for very low and very high duty cycles indicating that these cases are most probable. This result is not only valid for the shown frequency bands but for nearly all the technologies and frequency bands that we investigated.

Often not a single sample passes the detection threshold and $DC_i \equiv 0$. In contrast, a strong continuous signal as transmitted by, e.g, broadcasting stations, results in $DC_i \equiv 1$. For some systems also other technology characteristics increase the probabilities for the two extremes. The UMTS technology is based on Code Division Multiple Access (CDMA) and UMTS base stations transmit continuous signals in the downlink direction. If the received *PSD* is above the detection threshold DC_i will be one. The former case of $DC_i \equiv 0$ is due to unused UMTS channels and applies for $\approx 60\%$ of the UMTS band at NE. These are the reasons for the very flat UMTS-graph. If the received *PSD* is close to the detection threshold or noise samples are strong enough to cause false detections, intermediate duty cycles may also occur. In the UMTS case most of the rare intermediate values are due to one weak UMTS channel and the edges of all other UMTS signals present at NE.

The shown GSM900-graph is an example for a very busy band without any vacant channel. Since the graph corresponds to the more noisy radio environment at NE some of these channels might still be vacant but strong noise samples trigger false detections and result in intermediate duty cycles. As discussed for the UMTS-case also the results collected at AB indicate that both fully loaded and completely vacant channels often occur in the same band. While about 60% of the channels are never idle, 20% of the channels would be available for secondary use during the whole time period.

Distributions with high probabilities for the two extremes, $DC_i \approx 0$ and $DC_i \approx 1$, can usually be modelled well with the beta distribution, given by

$$f_b(x;\alpha,\beta) = \frac{1}{\mathbb{B}(\alpha,\beta)} x^{\alpha-1}(1-x)^{\beta-1}, \quad x \in (0,\ 1), \tag{3}$$

where α and β are two free parameters to control the behaviour of the distribution and $\mathbb{B}(\alpha,\beta)$ is the beta function

$$\mathbb{B}(\alpha,\beta) = \int_0^1 t^{\alpha-1}(-t)^{\beta-1} dt. \tag{4}$$

Additionally, the beta distribution can be flexibly configured in order to describe various different behaviours without the need to introduce another type of distribution. As discussed above, we found a significant number of channels with $DC_i \equiv 0$ or $DC_i \equiv 1$ in several of our measured traces. Since the beta distribution does never approach 0 or 1 we use a modified beta distribution for duty cycle modelling. Let $p_{DC=0}$ denote the probability of a completely idle channel and $p_{DC=1}$ denote the probability of a completely occupied channel, respectively. We define the modified beta distribution $f_{mb}(x;\alpha,\beta)$ as

$$\begin{aligned} f_{mb}(x;\alpha,\beta) = {} & p_{DC=0} \cdot \delta(x) \\ & + (1 - p_{DC=0} - p_{DC=1}) \cdot f_b(x;\alpha,\beta) \\ & + p_{DC=1} \cdot \delta(x-1), \quad x \in [0,\ 1], \end{aligned} \tag{5}$$

where $\delta(x)$ is the Dirac delta-function.

We will now use our measurement results and the estimated distribution functions to show that the

[8]The results presented in [32] have been computed using the whole measurement traces and kernel-based CDF estimation as offered by MATLAB. Here, we use representative subtraces that describe the daytime spectrum occupancy. Additionally, we use the empirical CDF since the kernel-based estimation does not accurately estimate steps in the CDF that may occur if single subbands show clearly different duty cycles.

modified beta distribution is a good model for the duty cycle distribution. We will apply two *goodness-of-fit* metrics to evaluate the accuracy of the distribution fits [33].[9] First, we use a reweighted version of the Kolmogorov-Smirnov (KS_w) metric as applied, e.g., in [9]:

$$KS_w(k) = \max_{k\in[1,J]} \frac{|F(k) - G(k)|}{\sqrt{G(k)(1-G(k))}}, \tag{6}$$

where F is the measured CDF, G is the CDF of the fitted model, and J denotes the number of bins used during the estimation of the CDF. We use the KS_w-metric because it is reweighted to consider also the differences at the extreme ranges of k appropriately.

Second, we apply an area-metric A as given, e.g., in [19]. It is defined as

$$\begin{aligned} A(F,G) = \frac{1}{J}\sum_{j=1}^{J} \left|\log(F^{-1}(j/J)) - \log(G^{-1}(j/J))\right| \\ - \frac{\left|\log(F^{-1}(1/J)) - \log(G^{-1}(1/J))\right|}{2J} \\ - \frac{\left|\log(F^{-1}(1)) - \log(G^{-1}(1))\right|}{2J}, \end{aligned} \tag{7}$$

The inverse function F^{-1} for a stepwise defined distribution function F can be defined as

$$F^{-1}(k) = \inf\{q : F(q) > k\}. \tag{8}$$

The inverse function G^{-1} is defined similarly.

Figure 6 repeats the four previously discussed CDF examples and also shows the corresponding modified beta distribution fits. Additionally, the results for the KS_w and A are given. All fits are sufficiently close to the measured distribution and prove that the modified beta distribution can reproduce the measured characteristics of the duty cycle. Especially, the explicit modelling of $p_{DC=0}$ and $p_{DC=1}$ results in good fits.

Table 3 lists all required parameters for the modified beta distribution for various services but also the lower two complete subbands. We also include the goodness-of-fit results in order to show how well each case could be modelled by the modified beta distribution. We list parameters for both calm radio environments at AB and IN and the busier environment at NE in order

[9]In [32] we applied the symmetric Kullback-Leibler divergence as goodness-of-fit metric. We switched to other metrics due to the characteristics of the applied CDF estimation. The kernel-based CDF estimation, as executed in [32], results in rather smooth curves but the empirical CDF is more realistic and reproduces further details, e.g., sharp steps. The Kullback-Leibler divergence is too sensitive to such characteristics and the other metrics turned out to be more robust for our application.

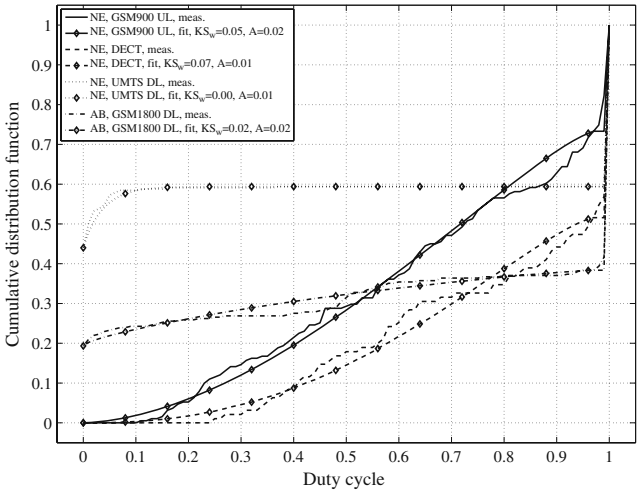

Fig. 6 Comparison of different duty cycle distributions and the corresponding modified beta distribution fits. The shown graphs are based on measurements taken at NE and AB using the same thresholds as given in Fig. 5

to enable scenario generation for different types of radio environments. Additionally, for the calm radio environments the better fit of the two options AB and IN and for the busier environment the better fitting threshold can be selected. The given parameters enable straightforward generation of realistic duty cycle data sets for DSA and cognitive radio research.

Few of the listed parameter sets result in higher values for the weighted Kolmogorov-Smirnov- or the area-metric. In most of these cases steps can be identified in the shape of the CDF due to similar duty cycles throughout wider communication channels. Such steps cannot be well reproduced by the beta distribution. However, since we do not want to model each wireless system separately but ensure a single and general model for the DC distribution we focus on the modified beta distribution.

4.2 Impact of the energy detection threshold

The energy detection threshold γ has significant impact on the duty cycle distribution. Figure 7 compares the distribution of DC_i as measured at the location IN. We estimated the distributions for all tested threshold values and used the data collected in the first subband. Although not listed in Table 3, all distributions could be represented well by the modified beta distribution as proven by the weighted KS-statistic and the area metric. The proposed model is applicable for all cases and is not sensitive to the energy detection threshold per se.

Table 3 Parameters of the modified beta distribution for duty cycle modelling

Data set	Location	Subband [MHz]	Threshold γ [dBm/200 kHz]	p_{DC0}	p_{DC100}	α	β	KS_w	A
Whole subband	AB	$f_c = 770$	−107	0.195	0.308	0.414	1.098	0.055	0.068
Whole subband	IN	$f_c = 770$	−107	0.480	0.222	0.597	1.044	0.012	0.013
Whole subband	NE	$f_c = 770$	−100	0.326	0.217	0.463	1.180	0.057	0.053
Whole subband	NE	$f_c = 770$	−107	0.001	0.515	0.761	1.004	0.066	0.044
TV	AB	$f_c = 770$	−107	0.189	0.342	0.414	1.103	0.047	0.068
TV	IN	$f_c = 770$	−107	0.459	0.058	0.520	1.622	0.057	0.049
TV	NE	$f_c = 770$	−100	0.455	0.208	0.389	1.226	0.057	0.062
TV	NE	$f_c = 770$	−107	0.000	0.409	0.801	1.121	0.074	0.057
GSM900 UL	AB	$f_c = 770$	−107	0.007	0.124	0.612	3.174	0.157	0.152
GSM900 UL	IN	$f_c = 770$	−107	0.825	0.015	0.473	3.197	0.043	0.028
GSM900 UL	NE	$f_c = 770$	−100	0.272	0.016	0.489	3.576	0.161	0.117
GSM900 UL	NE	$f_c = 770$	−107	0.000	0.267	1.750	1.252	0.046	0.017
GSM900 DL	AB	$f_c = 770$	−107	0.000	0.934	3.677	1.336	0.035	0.001
GSM900 DL	IN	$f_c = 770$	−107	0.044	0.401	0.575	1.528	0.072	0.057
GSM900 DL	NE	$f_c = 770$	−100	Too little data, the subband is nearly completely loaded.					
GSM900 DL	NE	$f_c = 770$	−107	Too little data, the subband is nearly completely loaded.					
Whole subband	AB	$f_c = 2250$	−107	0.879	0.039	0.620	3.127	0.016	0.009
Whole subband	IN	$f_c = 2250$	−107	0.875	0.036	0.412	1.090	0.021	0.014
Whole subband	NE	$f_c = 2250$	−100	0.747	0.065	0.452	1.886	0.037	0.029
Whole subband	NE	$f_c = 2250$	−107	0.424	0.151	0.425	1.209	0.063	0.064
GSM1800 UL	AB	$f_c = 2250$	−107	0.878	0.000	1.775	91.673	0.055	0.009
GSM1800 UL	IN	$f_c = 2250$	−107	Too little data, the subband is nearly completely vacant.					
GSM1800 UL	NE	$f_c = 2250$	−100	0.785	0.000	0.396	2.780	0.119	0.053
GSM1800 UL	NE	$f_c = 2250$	−107	0.324	0.046	0.396	1.703	0.155	0.136
GSM1800 DL	AB	$f_c = 2250$	−107	0.193	0.616	0.716	1.202	0.024	0.019
GSM1800 DL	IN	$f_c = 2250$	−107	0.344	0.111	0.698	1.317	0.040	0.027
GSM1800 DL	NE	$f_c = 2250$	−100	0.000	0.746	1.265	1.151	0.023	0.007
GSM1800 DL	NE	$f_c = 2250$	−107	0.000	0.949	16.465	1.923	0.046	0.001
DECT	AB	$f_c = 2250$	−107	0.073	0.000	1.688	4.927	0.124	0.060
DECT	IN	$f_c = 2250$	−107	0.418	0.000	1.955	63.373	0.109	0.036
DECT	NE	$f_c = 2250$	−100	0.011	0.211	1.110	3.227	0.079	0.043
DECT	NE	$f_c = 2250$	−107	0.000	0.484	2.454	1.352	0.067	0.015
UMTS UL	AB	$f_c = 2250$	−107	Too little data, the subband is nearly completely vacant.					
UMTS UL	IN	$f_c = 2250$	−107	Too little data, the subband is nearly completely vacant.					
UMTS UL	NE	$f_c = 2250$	−100	0.914	0.003	0.701	12.104	0.043	0.010
UMTS UL	NE	$f_c = 2250$	−107	0.157	0.012	0.478	2.369	0.203	0.132
UMTS DL	AB	$f_c = 2250$	−107	0.596	0.383	1.481	1.075	0.003	0.001
UMTS DL	IN	$f_c = 2250$	−107	0.611	0.188	0.868	1.344	0.023	0.010
UMTS DL	NE	$f_c = 2250$	−100	0.440	0.406	0.932	23.791	0.004	0.012
UMTS DL	NE	$f_c = 2250$	−107	0.120	0.511	0.349	0.632	0.075	0.076
ISM at 2.4 GHz	AB	$f_c = 2250$	−107	0.144	0.000	0.840	5.947	0.265	0.126
ISM at 2.4 GHz	IN	$f_c = 2250$	−107	0.654	0.000	0.521	12.113	0.248	0.100
ISM at 2.4 GHz	NE	$f_c = 2250$	−100	0.586	0.004	0.380	1.935	0.109	0.082
ISM at 2.4 GHz	NE	$f_c = 2250$	−107	0.193	0.162	0.447	2.635	0.088	0.123

In some subbands the duty cycles of only very few channels are different from $DC \approx 100\%$ or $DC \approx 0\%$. In these cases model parameters cannot be reliably estimated

Aside from the model accuracy different energy detection thresholds still result in significantly different distributions but, based on our measurement data, interference and primary user signals cannot be differentiated. This fact leaves us with the need to choose a detection threshold arbitrarily based on an estimation of the background noise floor. Often the detection threshold has been determined by comparison to the noise distribution as measured with a 50 Ω fitted match, see, e.g., [8] and [12], but in rather noisy radio environments, such as NE, these low detection thresholds will result in $DC_i = 1$ for numerous channels.

At the calm radio environment AB we received less primary user signals. At the same time the background

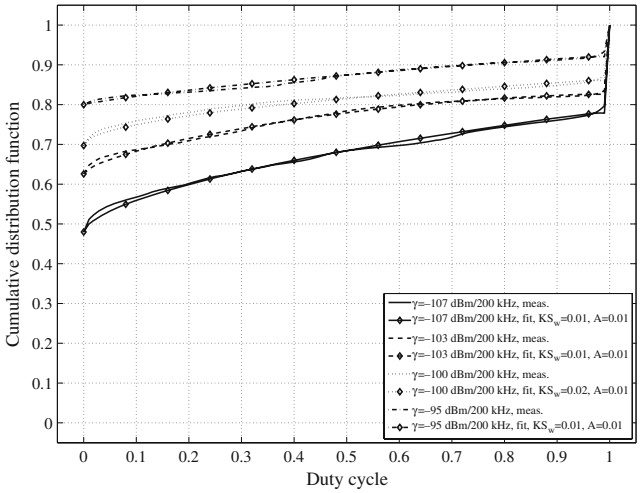

Fig. 7 Comparison of the impact of different energy detection thresholds on the duty cycle distributions and the modified beta distribution fits. The shown graphs are based on measurements taken in the whole first subband at IN

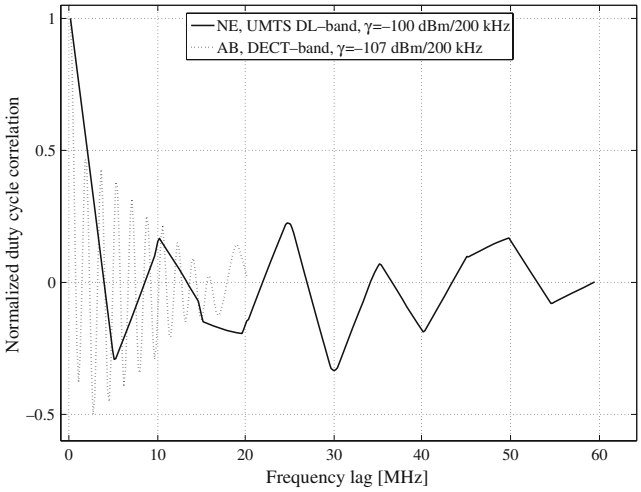

Fig. 8 Normalized correlation of the duty cycle plotted over the frequency lag for selected examples. The shown graphs are based on measurements taken at NE and AB using appropriate thresholds

noise process is weak enough such that all detected signals are due to intended primary user transmissions instead of unintended interference when using the threshold $\gamma = -107$ dBm/ 200 kHz, initially proposed by the IEEE 802.22 standardization committee. Therefore, the model parameters for AB definitely describe a realistic but calm radio environment.

4.3 Duty cycle correlation over frequency

Frequency agility is one of the core features of DSA-capable systems. Thus, for evaluation of DSA protocols or algorithms multiple adjacent channels should always be modelled. In this context, the question if the duty cycles of adjacent channels are correlated is important. Figure 8 shows the correlation of the measured DC_i plotted over the frequency lag for two selected services. For both examples, the Digital Enhanced Cordless Telecommunications (DECT) and the UMTS DL, the correlation characteristics and the system bandwidth are clearly interconnected. DECT signals cover about 1.7 MHz and are narrower than UMTS signals of 5 MHz bandwidth. Also the band allocated for the whole DECT service is narrower than the band assigned to the UMTS DL service.

The duty cycle is highly correlated for measurement channel indices belonging to the centre of the same or any of the neighbouring DECT channels. The correlation is lower or even negative for other frequency lags. In the case of UMTS no perfect periodicity as in the DECT case is present. Since DECT applies periodic and dynamic frequency selection all available ten channels are equally busy. In contrast, UMTS employs fixed frequency assignments and unused channels in between lower the correlation.

As the correlation of the duty cycle is dominated by the primary user signal bandwidth, realistic duty cycle modelling requires knowledge on the primary user bandwidth. The introduced duty cycle model does not consider the correlation, yet. However, since it is based on real life measurements and reproduces the probabilities well, it is still superior compared to models existing in the literature, e.g., [11].

We have provided a more detailed spectrum model that also takes into account correlation characteristics in the frequency domain in [33]. However, the required number of parameters and the model complexity are clearly higher. Thus, each researcher may decide upon the required model accuracy and appropriate complexity based on the application at hand.

5 Adaptive spectrum sensing

Fast and reliable identification of vacant spectrum is very important for efficient secondary system operation. Several researchers have evaluated the problem of how to choose the set of channels for sensing that maximizes the probability of finding sufficient amount of idle spectrum. The solutions presented in [18, 36] are examples for theoretical formulations of the problem and [11, 30, 31] are examples for more practically motivated approaches.

Here, we use the adaptive spectrum sensing as an example for relevant applications for the introduced spectrum model in DSA research. We elaborate on the importance of realistic spectrum modelling by comparing the efficiency of the same adaptive sensing algorithm when applied to spectrum occupancy data generated using different spectrum models or our measurement traces directly.

We assume an adaptive sensing algorithm that selects a subset of the available channels for sensing and analyse the probability that all sensed channels are idle. We focus on non-consecutive spectrum since we have seen in Section 4.3 that the correlation properties of the duty cycle over frequency are not accurately reproduced by our model.

We define B as a group of N channels selected for sensing:

$$B = \{b_1, \ldots, b_N\} \in W, \quad b_i \in [1,\ K], \tag{9}$$

where $b_1, \ldots, b_N$ are the selected channel indices and W denotes the whole subband under evaluation consisting of K channels. Then,

$$p_B = \prod_{i=1}^{N} (1 - DC_{b_i}), \tag{10}$$

is the probability that all channels in the group B will be idle at the same time.

The adaptive sensing algorithm is in charge of identifying the optimal group $\hat{B}$ of N channels that maximises p_B:

$$\hat{B} = max_{B \in W} p_B. \tag{11}$$

5.1 Duty cycle based sensing

We evaluate the following adaptive sensing algorithm: The scheme exploits knowledge of the DC_i for each channel i and selects those channels with lowest DC_i for sensing [31].

Our analysis is focused on the impact of the DC distribution on the sensing performance. Thus, we do not consider more advanced schemes that exploit knowledge on the distributions of idle- and busy-periods for each channel as discussed in, e.g., [18].

Let $\tilde{b}_1 \ldots \tilde{b}_N$ denote the channel indices of those N channels with the lowest DC_i selected for sensing. Following the DC-based sensing algorithm it will be optimal to limit sensing to those N channels. Hence, the main performance metric for evaluation is

$$p_{\hat{B}}(N) = \prod_{i=1}^{N} (1 - DC_{\tilde{b}_i}). \tag{12}$$

5.2 Artificial spectrum models

We compare the following three artificial spectrum models:

1. *Constant DC*:
   The duty cycle is same for each channel:
   $DC_i = \overline{DC} = 0.25$.
2. *Uniform DC*:
   The duty cycle is uniformly distributed [11]:
   $DC_i = U\ [0,\ 2x\overline{DC}] = U\ [0,\ 0.5]$.
3. *Modified beta distribution*:
   The duty cycle is modelled using the modified beta distribution as introduced in Section 4.1:
   $p_{DC=0} = 0.1$, $p_{DC=1} = 0.1$, $\alpha = 0.5$, and $\beta = 2.167$.

All models result in the same average duty cycle $\overline{DC} = 0.25$ over the whole examined subband.

Figure 9 compares the efficiency of the DC-based sensing when evaluated with spectrum occupancy data generated from the three introduced models. We generated occupancy data for subbands of $K = 500$ channels and averaged the results over ten simulation runs. The standard deviations over the simulation runs are negligible and are not shown in Fig. 9. The performance estimated based on the spectrum occupancy generated using the modified beta distribution is clearly better compared to the two other models. The configured 10 % of completely vacant channels are detected by the sensing algorithm and about 60–70 idle channels can be identified with very high probability.

The impact of the different spectrum models is significant. The uniform distribution results in too few channels with very low DC that are the most attractive channels for DSA. The model with constant DC also

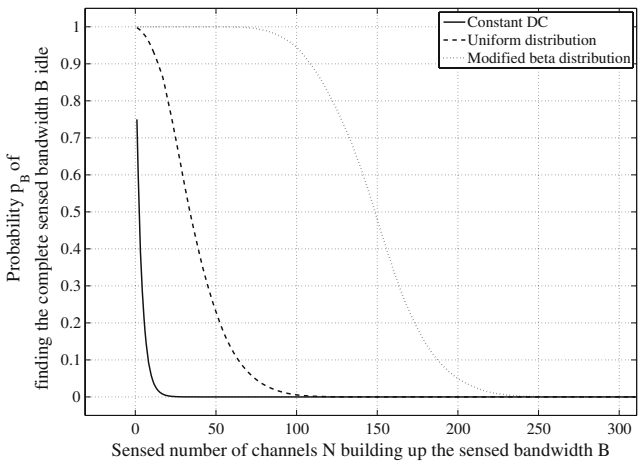

Fig. 9 Comparison of the probability $p_{\hat{B}}$ to find the complete sensed band $\hat{B}$ idle computed for various artificial DC-models

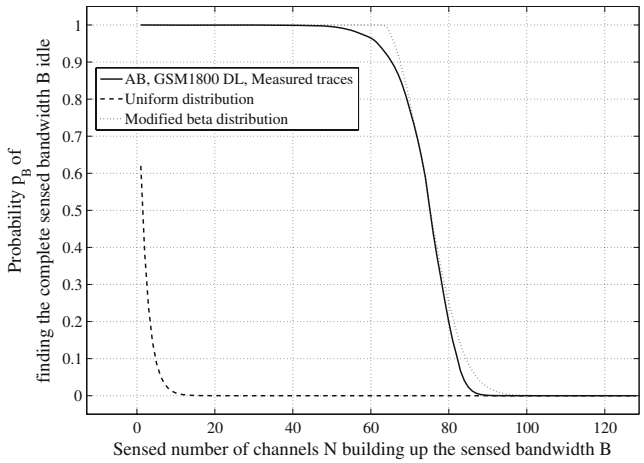

Fig. 10 Comparison of the probability $p_{\hat{B}}$ to find the complete sensed band $\hat{B}$ idle computed for selected artificial *DC*-models and traces measured at AB

gives a wrong impression of the sensing performance. These results show that also from an application point of view accurate reproduction of the two extreme cases of fully loaded and completely vacant channels is of special interest. Our introduced model enables realistic spectrum modelling and reliable evaluation of different sensing algorithms.

5.3 Comparison to measurement data

Finally, we compare the performance of the adaptive sensing algorithm when applying it to measured spectrum occupancy traces or spectrum data as generated from different models.

Figure 10 shows the same type of graph as discussed in the previous Section. The results for the measured traces, taken from the GSM1800 downlink band data collected at AB, and the appropriately fitted modified beta distribution are very similar. Again, the result for the uniform distribution is significantly different. The slight differences between the measured traces and our model are due to small model inaccuracies that we consider as acceptable because the same model structure can be applied to various different wireless technologies without modification. At the price of higher model complexity also more accurate reproduction can be achieved as investigated, e.g., in [33].

6 Conclusion

In this paper we have discussed our spectrum occupancy measurement setup in detail and have elaborated on the major design decisions and lessons learned. We have presented a comparison of three measurement locations. Not only the signal strength received from active transmitters but also the intensity of the background noise processes varies between locations. At the more exposed and centrally located site higher noise levels could be measured.

In a second step we have introduced a new model for the duty cycle distribution. Based on our extensive measurement results we have shown that the cases of completely busy or vacant channels are very probable and modified the beta distribution to reproduce these characteristics. We have demonstrated that the proposed model fits well and have listed model parameters for multiple wireless systems.

The presented duty cycle model is beneficial for multiple applications in the evaluation of dynamic spectrum access systems. As an example use case for the model we have examined the performance of adaptive spectrum sensing when evaluated using spectrum occupancy data generated from various spectrum models. Again, we have shown the importance of accurate reproduction of the special cases of fully loaded or completely idle channels. Our model has provided very similar results as extracted from the measurement traces directly, which validates the pursued modelling approach.

In our future work we will investigate further adaptive sensing algorithms. The measurement data is available to the research community from http://download.mobnets.rwth-aachen.de.

Acknowledgements The authors would like to thank the RWTH Aachen University and the German Research Foundation (Deutsche Forschungsgemeinschaft, DFG) for providing financial support through UMIC research centre. We would also like to thank the European Union for providing partial funding of this work through the ARAGORN project. Additionally, we would like to thank the International School Maastricht, Maastricht, Netherlands, and Marten Bandholz and Sonja Bone for providing us access to the outdoor measurement locations. Finally, we would like to thank Jin Wu and Gero Schmidt-Kärst for their support during the measurements.

References

1. Agilent Technologies (2006) PSA series spectrum analyzers, data sheet
2. Akyildiz IF, Lee WY, Vuran MC, Mohanty S (2006) Next generation/dynamic spectrum access/cognitive radio wireless networks: a survey. Comput Networks (Elsevier) 50(13):2127–2159
3. Bacchus RB, Fertner AJ, Hood CS, Roberson DA (2008) Long-term, wide-band spectral monitoring in support of dynamic spectrum access networks at the IIT Spectrum

Observatory. In: Proc. of 3rd IEEE symposium on new frontiers in dynamic spectrum access networks (DySPAN), Chicago
4. Blaschke V, Jäkel H, Renk T, Klöck C, Jondral FK (2007) Occupation measurements supporting dynamic spectrum allocation for cognitive radio design. In: Proc. of international conference on cognitive radio oriented wireless networks and communications (CROWNCOM), Orlando, pp 50–57
5. Brandes S, Cosovic I, Schnell M (2006) Reduction of out-of-band radiation in OFDM systems by insertion of cancellation carriers. IEEE Commun Lett 10(6):420–422
6. Brodersen RW, Wolisz A, Cabric D, Mishra SM, Willkomm D (2004) White paper: CORVUS—a cognitive radio approach for usage of virtual unlicensed spectrum. Tech. rep., University of California, Berkeley. http://bwrc.eecs.berkeley.edu/Research/MCMA/CR_White_paper_final1.pdf. Accessed 18 May 2009
7. Cabric D, Tkachenko A, Brodersen RW (2006) Experimental study of spectrum sensing based on energy detection and network cooperation. In: Proc. of workshop on technology and policy for accessing spectrum (TAPAS), Boston
8. Chiang RIC, Rowe GB, Sowerby KW (2007) A quantitative analysis of spectral occupancy measurements for cognitive radio. In: Proc. of IEEE vehicular technology conference (VTC), Dublin, pp 3016–3020
9. Clauset A, Shalizi CR, Newman MEJ (2009) Power-law distributions in empirical data. Society for Industrial and Applied Mathematics (SIAM) Review (SIREV)
10. Cosovic I, Brandes S, Schnell M (2006) Subcarrier weighting: a method for sidelobe suppression in OFDM systems. IEEE Commun Lett 10(6):444–446
11. Datla D, Rajbanshi R, Wyglinski AM, Minden GJ (2007) Parametric adaptive spectrum sensing framework for dynamic spectrum access networks. In: Proc. of IEEE symposium on new frontiers in dynamic spectrum access networks (DySPAN), Dublin, pp 482–485
12. Ellingson SW (2005) Spectral occupancy at VHF: implications for frequency-agile cognitive radios. In: Proc. of IEEE vehicular technology conference (VTC), vol 2, Dallas, pp 1379–1382
13. Geirhofer S, Tong L, Sadler BM (2007) Dynamic spectrum access in the time domain: modeling and exploiting white space. IEEE Commun Mag 45(5):66–72
14. Haykin S (2005) Cognitive radio: brain-empowered wireless communications. IEEE J Sel Areas Commun 23(2): 201–220
15. Holland O, Cordier P, Muck M, Mazet L, Klöck C, Renk T (2007) Spectrum power measurements in 2G and 3G cellular phone bands during the 2006 football world cup in Germany. In: Proc. of IEEE symposium on new frontiers in dynamic spectrum access networks (DySPAN), Dublin, pp 575–578
16. Islam M, Koh C, Oh S, Qing X, Lai Y, Wang C, Liang YC, Toh B, Chin F, Tan G, Toh W (2008) Spectrum survey in Singapore: occupancy measurements and analyses. In: Proc. of international conference on cognitive radio oriented wireless networks and communications (CROWNCOM). Singapore
17. Mitola J III (2000) Cognitive radio: an integrated agent architecture for software defined radio. Ph.D. thesis, KTH (Royal Institute of Technology), Stockholm
18. Kim H, Shin KG (2008) Efficient discovery of spectrum opportunities with MAC-layer sensing in cognitive radio networks. IEEE Trans Mob Comput 7(5):533–545
19. Köpke A, Willig A, Karl H (2003) Chaotic maps as parsimonious bit error models of wireless channels. In: Proc. of IEEE conference on computer communications (INFOCOM), vol 1, San Francisco, pp 513–523
20. McHenry MA (2005) NSF spectrum occupancy measurements project summary. Tech. rep., Shared Spectrum Company
21. McHenry MA, McCloskey D (2006) Multi-band, multi-location spectrum occupancy measurements. In: Proc. of international symposium on advanced radio technologies (ISART), Boulder, pp 167–175
22. McHenry MA, Tenhula PA, McCloskey D, Roberson DA, Hood CS (2006) Chicago spectrum occupancy measurements & analysis and a long-term studies proposal. In: Proc. of workshop on technology and policy for accessing spectrum (TAPAS), Boston
23. Pagadarai S, Rajbanshi R, Wyglinski A, Minden G (2008) Sidelobe suppression for OFDM-based cognitive radios using constellation expansion. In: Proc. of IEEE wireless communications and networking conference (WCNC), Las Vegas, pp 888–893
24. Petrin A, Steffes PG (2005) Analysis and comparison of spectrum measurements performed in urban and rural areas to determine the total amount of spectrum usage. In: Proc. of international symposium on advanced radio technologies (ISART), Boulder, pp 9–12
25. Polastre J, Szewczyk R, Culler D (2005) Telos: enabling ultra-low power wireless research. In: Proc. of international symposium on information processing in sensor networks (IPSN), special track on platform tools and design methods for network embedded sensors (SPOTS), Los Angeles, pp 364–369
26. Roberson DA (2007) Structural support for cognitive radio system deployment. In: Proc. of international conference on cognitive radio oriented wireless networks and communications (CROWNCOM), Orlando, pp 401–407
27. Rogers AEE, Salah JE, Smythe DL, Pratap P, Carter JC, Derome M (2005) Interference temperature measurements from 70 to 1500 MHz in suburban and rural environments of the Northeast. In: Proc. of IEEE symposium on new frontiers in dynamic spectrum access networks (DySPAN), Baltimore, pp 119–123
28. Sanders FH (1998) Broadband spectrum surveys in Denver, CO, San Diego, CA, and Los Angeles, CA: methodology, analysis, and comparative results. In: Proc. of IEEE symposium on electromagnetic compatibility, vol 2, Denver, pp 988–993
29. Shellhammer S, Chouinard G (2006) Spectrum sensing requirements summary. IEEE 802.22-05/22-06-0089-05-0000
30. Wellens M, de Baynast A, Mähönen P (2008) Exploiting historical spectrum occupancy information for adaptive spectrum sensing. In: Proc. of IEEE wireless communications and networking conference (WCNC), Las Vegas, pp 717–722
31. Wellens M, de Baynast A, Mähönen P (2008) On the performance of dynamic spectrum access based on spectrum occupancy statistics. IET Communications, Special Issue on Cognitive Spectrum Access 2(6):772–782
32. Wellens M, Mähönen P (2009) Lessons learned from an extensive spectrum occupancy measurement campaign and a stochastic duty cycle model. In: Proc. of international conference on testbeds and research infrastructures for the development of networks and communities (Tridentcom), Washington, D.C.
33. Wellens M, Riihijärvi J, Mähönen P (2009) Empirical time and frequency domain models of spectrum use. Phys Comm, Special Issue on Cognitive Radio: Algorithms & System Design (Elsevier) 2(1–2):10–32

34. Wellens M, Wu J, Mähönen P (2007) Evaluation of spectrum occupancy in indoor and outdoor scenario in the context of cognitive radio. In: Proc. of international conference on cognitive radio oriented wireless networks and communications (CROWNCOM), Orlando, pp 420–427
35. Zhao Q, Sadler B (2007) A survey of dynamic spectrum access. IEEE Signal Process Mag 24(3):79–89
36. Zhao Q, Tong L, Swami A, Chen Y (2007) Decentralized cognitive MAC for opportunistic spectrum access in ad hoc networks: a POMDP framework. IEEE J Sel Areas Commun 25(3):589–600